Universiteit
Leiden
The Netherlands

Absorption, luminescence and scattering of single nano-objects

Yorulmaz, M.

Citation

Yorulmaz, M. (2013, June 26). *Absorption, luminescence and scattering of single nano-objects*. *Casimir PhD Series*. Retrieved from https://hdl.handle.net/1887/21018

Version:	Not Applicable (or Unknown)
License:	Licence agreement concerning inclusion of doctoral thesis in the Institutional Repository of the University of Leiden
Downloaded from:	https://hdl.handle.net/1887/21018

Note: To cite this publication please use the final published version (if applicable).

Cover Page

Universiteit Leiden

The handle http://hdl.handle.net/1887/21018 holds various files of this Leiden University dissertation

Author: Yorulmaz, Mustafa
Title: Absorption, luminescence, and scattering of single nano-objects
Issue Date: 2013-06-26

CHAPTER 2

Room-temperature detection of a single molecule's absorption by photothermal contrast

So far, single-molecule imaging has predominantly relied on fluorescence detection. We imaged single nonfluorescent azo dye molecules in room-temperature glycerol by the refractive effect of the heat that they release in their environment upon intense illumination. This photothermal technique provides contrast for the absorbing objects only, irrespective of scattering by defects or roughness, with a signal-to-noise ratio of $\sim$10 for a single molecule in an integration time of 300 milliseconds. In the absence of oxygen, virtually no bleaching event was observed, even after more than 10 minutes of illumination. In a solution saturated with oxygen, the average bleaching time was of the order of 1 minute. No blinking was observed in the absorption signal. On the basis of bleaching steps, we obtained an average absorption cross section of 4 $Å^2$ for a single chromophore.

The contents of this chapter are based on:
A. Gaiduk, M. Yorulmaz, P. V. Ruijgrok, and M. Orrit, "Room-temperature detection of a single molecule's absorption by photothermal contrast", Science **330**, 353-356 (2010) and A. Gaiduk, P. V. Ruijgrok, M. Yorulmaz, and M. Orrit, "Detection limits in photothermal microscopy", Chem. Sci. **1**, 343-350 (2010)

2.1 Introduction

Single-molecule optical detection[47] has become an indispensable tool in molecular biology and materials science. For the past 20 years, optical single-molecule detection has relied on fluorescence[33,122] because of the low background of this technique. However, monitoring optical absorption more directly would have definite advantages. Fluorescence requires an efficient pathway for populating the emitting state and also the near absence of nonradiative relaxation to the ground state or to intermediate dark states. The fluorescent state is easily destroyed or quenched by photochemical reactions, often involving electron or proton transfer. Indeed, only a very small fraction of all absorbing molecules (called chromophores) are strongly fluorescent (then called fluorophores). Nonfluorescent chromophores include certain metal complexes and many conjugated molecules, for example, DNA bases, that are important in biology. Such molecules could become more natural labels than fluorophores.

The first single-molecule optical detection experiment, by Kador and Moerner, was achieved by absorption[100] but relied on favorable cryogenic conditions, under which the absorption cross section of the narrowest molecular transition was extremely large. Their doubly modulated absorption technique was later improved on with modern optics and detectors,[101–103] but the absorption signal still appears on a strong background of unabsorbed photons, resulting in a lower signal-to-noise ratio than fluorescence. Detecting the absorption of a single molecule at ambient conditions is much more challenging than at low temperature because of the reduction by 5 to 6 orders of magnitude of the cross section, essentially because of fast dephasing by thermal fluctuations. A method for the detection of single-molecule absorption at room temperature must thus solve two different problems.

First, the absorption cross section of a typical chromophore at room temperature is only of the order of 10^{-2} nm^2. The number of the absorption events varies as the ratio of the absorption cross section to the area of a diffraction-limited light beam. This ratio is about 10^{-7} for a laser spot diameter of 300 nm. Because statistical fluctuations in a number N of photons are of order $\sqrt{N}$, a change in transmitted signal of 10^{-7} requires more than 10^{14} photons to be detected. Of those, at least 10^7 have to be absorbed by the molecule. The detection of such small signals therefore requires many

absorption events, which may conflict with the poor photostability of many fluorescent molecules at ambient conditions.

Second, in a direct extinction measurement, where only missing photons are identified, a molecule's absorption appears on a background of scattering by any inhomogeneities in refractive index, arising for instance from roughness of the interfaces. Therefore, for practical applications, it is vital to be able to discriminate true absorption from scattering.

Three main routes have been pursued in the past 10 years toward surmounting these obstacles.

Photothermal contrast relies on the intensity change of a probe beam caused by a modulated heating beam of a different color. Kitamori and coworkers[97] have detected sub-yoctomole concentrations of absorbers in solution with integration times of several seconds, that is, in conditions under which many diffusing molecules contributed in turn to the signal. Boyer et al.[38] applied a similar method to detect single immobilized gold nanoparticles down to 5 nm in diameter, a performance that was later substantially improved by Berciaud et al.[39,95] and has led to a number of applications in recent years.

Alternatively, various sensitive optical techniques have been applied either in interferometers[93] or in a reflection or transmission geometry[40,123] to detect some tens of molecules,[93] small particles,[40] or quantum dots.[88] In the latter two cases, however, the use of ultraclean and stable conditions was essential to ensure the absence of scattering background.

Most recently, Xie and co-workers have explored stimulated emission to distinguish absorption from scattering.[94] Indeed, because stimulated photons can only arise from the excited state of molecules, this method efficiently rejects scattering and fulfills the second requirement. With a modulated stimulating beam, they were able to image absorption in cells down to a few tens of molecules.

In this chapter, we push the sensitivity of photothermal detection to the single-molecule limit. We first discuss the photothermal method and examine the factors influencing the signal and the noise in photothermal detection. We then discuss the ways of improving the signal-to-noise ratio in photothermal microscopy experiments. Finally we demonstrate the detection of nonfluorescent molecules (BHQ1-10T-BHQ1 and BHQ1-Amine) by their absorption with a signal-to-noise ratio of about 10 with reasonable integration times

of 100 to 300 ms.

2.2 Photothermal detection

Photothermal detection is sensitive to the amount of energy absorbed by a nanoobject and dissipated as heat into its local environment. We define as the dissipated power P_{diss} the power provided by the heating beam (with power P_{heat}), which is dissipated as heat by the absorber. The heating-beam intensity is modulated at an angular frequency Ω. Therefore, we call P_{diss} the maximum instantaneous value of this power during the modulation period and the time-averaged dissipated power is $P_{\text{diss}}/2$.

The dissipated power results in a temperature profile $\Delta T(r,t)$ around the nanoabsorber in its embedded medium with thermal conductivity κ and heat capacity per unit volume C_{p}. This temperature profile $\Delta T(r,t)$ in steady conditions with sinusoidal modulation, is given by:[38]

$$\Delta T(r,t) = \frac{P_{\text{diss}}}{4\pi\kappa r}[1 + exp(-r/r_{\text{th}}) \times \cos(\Omega t - r/r_{\text{th}})] \tag{2.1}$$

where r is the distance from the center of the nanoabsorber and $r_{\text{th}} = \sqrt{2\kappa/\Omega C_{\text{p}}}$ is the length characterizing the damping of the heat waves in the medium.

Assuming the response to be instantaneous, this temperature profile in turn causes a refractive index profile $\Delta n(r,t) = \Delta T(r,t) \times \partial n/\partial T$ in the medium, acting as a modulated thermal nanolens.[98] A probe beam is used to detect that nanolens. In the usual photothermal geometry[39,97,98] the scattered probe field $E_{\text{sc}}(\text{t})$ interferes with a reference probe field E_{ref} (usually the transmitted beam or a reflection), and the resulting intensity $I_{\text{det}} \propto |\mathbf{E}_{\text{ref}} + \mathbf{E}_{\text{sc}}|^2$ is detected. In this discussion, we neglect the difference in spatial modes of the two fields, which are supposed to be similar. The lock-in amplifier isolates the weak contribution of the interference signal $2\text{Re}\left[E^*_{\text{ref}} E_{\text{sc}}(t)\right]$ modulated at the same frequency as the heating beam. The contribution of the modulated scattered intensity $|\mathbf{E}_{\text{sc}}|^2$ is neglected for small particles (typically < 60 nm).[42] For larger particles, a non-negligible static scattered field acts as an additional in-phase reference field. Its contribution to the interference intensity I_{det} is reported in photothermal correlation spectroscopy experiments for 80 nm gold particles.[124]

The photothermal signal S is proportional to the field scattered by an effective volume V where the refractive index is modulated. The refractive index change Δn depends on the absorption cross section σ_{abs} of the nano-object and the heating beam with intensity I_{heat} focused into a diffraction-limited spot with area A. Δn is proportional to the power dissipated by the nano-object $P_{\text{diss}} = I_{\text{heat}}\sigma_{\text{abs}} = \sigma_{\text{abs}}P_{\text{heat}}/A$. The field scattered by the thermal lens can be approximated by that of an equivalent dipole $|\mathbf{p}| \approx 2n\Delta n \cdot V \cdot \left|\mathbf{E}_{probe}\right|$, where $\Delta n \cdot V$ stands for the volume integral of the position-dependent refractive index change of the lens. The scattered field is radiated by this dipole: $|\mathbf{E}_{\text{sc}}(t)| \approx \frac{1}{4\pi\varepsilon_0\omega_0\lambda^2}|\mathbf{p}|$, and the photothermal signal can then be written as an optical power:

$$S \approx \frac{1}{\pi\omega_0} n \frac{\partial n}{\partial T} \frac{1}{C_p \lambda^2 \Omega} \frac{\sigma_{abs}}{A} P_{heat} P_{probe} \Delta t \tag{2.2}$$

where ω_0 is the probe beam focal radius (beam waist), C_p is the heat capacity per unit volume of the photothermal medium (for example, C_p for glycerol is 2.6×10^6 $\text{Jm}^{-3}\text{K}^{-1}$), λ and P_{probe} are the wavelength and power of the probe beam, and Δt is the integration time of the lock-in amplifier. We assume the thermal conductivity of metal nanoparticles to be much larger than that of the surrounding media (for example, $\kappa_{\text{gold}} = 310$ $\text{Wm}^{-1}\text{K}^{-1}$, $\kappa_{\text{water}} = 0.56$ $\text{Wm}^{-1}\text{K}^{-1}$).

The noise in actual experiments arises from the detector, from fluctuations of the probe laser power, and from photon noise of the detected optical power. In practice, the experimental noise is always larger than the photon noise, but can be close to it for an optimized setup. Here, assuming an ideal detector and a shot-noise limited detection, the noise N_s on the photothermal signal S would be:

$$N_s \propto \sqrt{\frac{P_{probe}\Delta t}{h\nu}} \tag{2.3}$$

Combining the expressions for the signal and the noise, we see that the signal-to-noise ratio SNR for the shot-noise-limited photothermal detection is given by:

$$SNR \approx \frac{1}{\pi\omega_0\lambda^2\Omega} n \frac{\partial n}{\partial T} \frac{1}{C_p} \frac{\sigma_{abs}}{A} P_{heat} \sqrt{\frac{P_{probe}\Delta t}{h\nu}} \tag{2.4}$$

2.3 Optimizing the SNR in photothermal detection

Here, we discuss how the SNR can be optimized by tuning all factors in Eq. 2.4, and we point out the practical limits to the optimization.

1. Increase the dissipated power up to the allowed maximum, usually fixed by saturation. For gold nanoparticles, the applicable powers are very high (the bulk melting temperature of gold is about 1300 K, and the temperature rise to reshape gold nanorods, although significantly lower[68,69,125] is still some hundreds of K). The allowed temperatures in biological samples, however, will be much lower. The melting intensity for a spherical particle with diameter 20 nm in water is around 20 MW/cm^2 at 514 nm (about 20 mW focused on a diffraction limited spot), and scales with R^{-2}. For a non-fluorescent molecule, the saturation intensity is determined mostly by the excited state lifetime τ, typically 0.1 ns, which leads to a dissipated power of a few nW.
2. Increase P_{probe} as much as possible. Practical limits are set by the maximum available laser power and by residual absorption of the probe beam by the sample. For example, the probe intensity can be increased until the probe-induced and pump-induced heating are comparable. For small gold NPs in glycerol, for example, we can use up to 125 times more probe intensity at 800 nm than heating intensity at 514 nm, as given by the ratio of the absorption cross sections.
3. Match the heat diffusion length r_{th} with the spot size, by choosing the right modulation frequency.[38,95] A lower modulation frequency generally leads to a higher photothermal signal, until the thermal lens exceeds the size of the focused probe beam. The optimal value of the modulation frequency also depends on the experimental noise spectrum.
4. Optimize the optical and thermal properties of the photothermal medium, including refractive index, its derivative with respect to temperature, heat capacity and conductivity.
5. Reduce the reflected intensity to reduce the laser noise by matching the indices of the substrate and the photothermal medium. (Only in reflection geometry.)

6. Increase the integration time of the lock-in amplifier. This parameter can be increased arbitrarily, provided the mechanical stability of the experimental setup and the photostability of the sample allow it.

2.4 Experiment

2.4.1 Samples

In this section we discuss how the samples were prepared for photothermal microscopy experiments. We firstly describe how we cleaned the glass slides. Then we explain how we prepared samples with single gold nanoparticles and single azo dyes.

Glass coverslides cleaning

Cleanliness of substrates and liquid is very important. There are many more absorbing molecules than fluorescent ones. The background problems become severe unless enough attention is paid to obtain a sample free from impurities.

Glass coverslides (Menzel, Germany) were cleaned in several successive sonication steps of 20 min in each of the following liquids: 2 % Hellmanex water solution, acetone, ethanol (AR grade), and Milli-Q water. Experiments were performed in a fluid cell (approx. $50 - 150$ μL volume) made from a rubber o-ring or a top of plastic Eppendorf tube attached to the coverslip. Clean glycerol ($> 99.5\%$, spectrophotometric grade) and hexane (AR grade) were used for experiments.

Gold nanoparticles

We used gold nanoparticles to characterize the sensitivity of our setup in absorption measurements. Gold nanoparticles provide good photostability and do not show saturation effects.

Samples of gold nanoparticles with diameters of 20, 10 and 5 nm (British Biocell International, EM.GC20) were prepared by dilution in ultra-pure water at volume ratios of 1:4, 1:20 and 1:25 respectively. Approximately 50 μL of the suspension were deposited on the surface of cleaned glass immediately after the filtration through a 450 nm porous membrane and spin coated at

2000 rpm for 5 s, followed by drying at 4000 rpm for 90 sec.

Black-Hole-Quenchers®

We selected a non-fluorescent azo dye which has a low quantum yield and a large dissipated power at saturation for photothermal detection.

Constructs of DNA with Black-Hole-Quenchers® (BHQ) were purchased from Eurogentech. Two BHQ1 molecules (BHQ1-10T-BHQ1) are about 3 − 4 nm apart as defined by the length of single-stranded DNA (ssDNA) primer (10T = 10 thymine nucleobases). The BHQ1-10T-BHQ1 construct shows maximum absorption at 520 nm in water and at about 530 nm in glycerol (see Fig. 2.1). The absorption of the construct at 514 nm is 1.6 times higher in glycerol than in water.

In order to prepare samples of DNA constructs for optical microscopy experiments, we spin-coated approximately 50 μL of the 10 nM aqueous solution of DNA constructs on the surface of clean glass slides at 2000 rpm for 5 s which was followed by drying at 4000 rpm for 90 s.

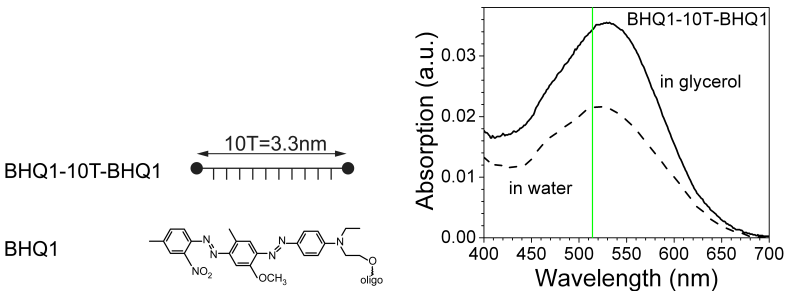

Figure 2.1: (Left) Schematic representation of the DNA construct (BHQ1-10T-BHQ1) and chemical structure of Black-Hole-Quencher (BHQ1) molecule. (Right) Absorption spectra of BHQ1-10T-BHQ1 construct in water (dashed) and in glycerol (solid) showing maximum absorption at 520 nm and at about 530 nm, respectively.

A batch of Black-Hole-Quencher® (BHQ1-Amine, $C_{24}H_{29}N_7O_3$, M_w = 475 Da) was purchased from Biosearch technologies, Inc. The absorption spectra of BHQ1-Amine molecules in water and in glycerol are shown in Fig. 2.2. For single-molecule absorption measurements, BHQ1-Amine molecules were deposited on the clean glass surface in the same way as DNA constructs sample.

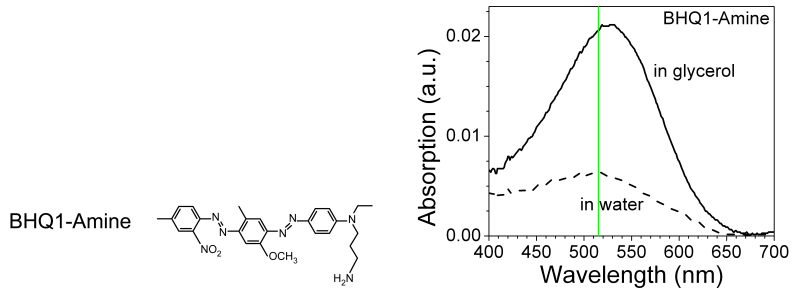

Figure 2.2: (Left) Schematic representation of the BHQ1-Amine molecule. (Right) Absorption spectra of BHQ1-Amine molecules in water (dashed) and in glycerol (solid) showing maximum absorption at 520 nm and at about 530 nm, respectively.

A chromophore that efficiently absorbs light and converts the absorbed energy efficiently into heat would be a good candidate for demonstration of room-temperature detection of a single molecule's absorption. In addition, the photochemical stability of the molecule is important and the molecule should resist bleaching for a long period.

The extinction coefficient of BHQ1 at the absorption maximum ($\sim$ 520 nm) in water is 34000 $M^{-1}cm^{-1}$. We assume the fluorescence lifetime of BHQ1 is 50 ps or less. The fluorescence lifetime of similar azo dyes was measured to be about 2 ps in various solvents[126] and several tens of ps in a polymer matrix[127].

2.4.2 Photothermal microscopy setup

The experimental setup is based on an inverted optical microscope, Olympus IX71, equipped with Olympus 60$\times$ oil immersion objective (NA = 1.45). The schematic of the setup is shown in Fig. 2.3. The heating beam is provided by an Ar-ion laser (Coherent Innova 300) and passes the acousto-optical modulator with a typical modulation frequency of about 1 MHz. The absorbed power provided by the heating beam gives rise to a temperature gradient (see Eq. 2.1) with an amplitude $\Delta T_{surf} = \frac{\sigma_{abs} I_{heat}}{4\pi\kappa R}$ at the surface of the source, assumed to be spherical: σ_{abs} is the absorption cross section of the absorber, I_{heat} the pump intensity, κ the thermal conductivity of the medium, and R the radius of the heat source. The probe beam at 800 nm is produced by a Ti:sapphire laser (S3900s, Spectra Physics) pumped with the Ar-ion laser.

Sets of spatial filters and telescopes expand initial beams to $\sim$ 20 mm to overfill the entrance pupil of the microscope objective ($\sim$ 10 mm). The beams are overlapped at a dichroic mirror and sent towards the objective. The photothermal signal is collected in the back-scattered mode and detected by a Si photodiode with an adjustable gain (DHPCA-100-F, Femto) and fed into the lock-in amplifier. The experiment is controlled with a home-written LabView software, and the data are collected by an acquisition card (ADWin Gold). The raster scanning of the samples is performed with a 3-axis piezostage (MARS II, Physik Instrumente).

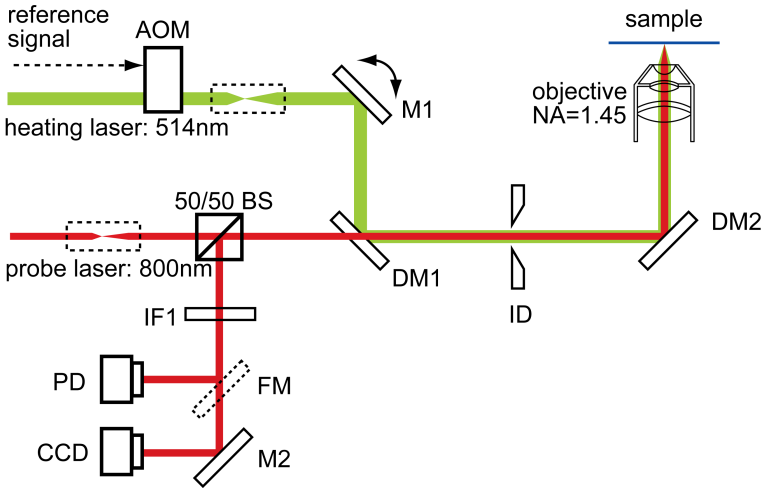

Figure 2.3: Scheme of the experimental setup for simultaneous photothermal detection. AOM - acousto-optical modulator, M - mirrors (scanning M1 is used for the control of the transversal alignment of the heating and probe beams), FM - flip mirrors, BS - beam splitter, DM - dichroic mirrors, ID - iris diaphragm, IF - interference filters, PD - photodiode, CCD - video cameras. Positions of beam-expanding telescopes are indicated with dashed boxes. Spatial filters are not shown in this schematic representation.

The photothermal signal is proportional to both the heating and probe powers. We modulate the heating beam at rather high frequency (around 1 MHz) to reject mechanical, electronic, and laser noise. In addition, we have chosen the reflection geometry with index matching to adapt the probe signal to the characteristics of our fast low-noise detector (maximum detected intensity 18 μW). A weak reflection of about 10^{-4} was obtained by using glycerol as the photothermal liquid ($n_{glyc.} = 1.47$) on top of a substrate of

cover glass ($n_{subs.} = 1.52$). With this near index match, very high probe intensities become applicable and the photon noise on the probe beam is therefore considerably reduced.

A near overlap of the two tightly focused beams with different colors that would yield maximum photothermal signal is also very critical. The photothermal signal was maximized by careful compensation of chromatic aberrations with the help of separate telescopes for different colors (dashed boxes in Fig. 2.3). A fast steering mirror (M1 in Fig. 2.3) was also used for transversal movement of the heating beam to check for the transversal overlap of the heating and probe beams.

2.5 Characterization of photothermal detection sensitivity on gold nanoparticles

We used our photothermal microscopy setup to improve the photothermal detection approach of Berciaud et al.[39,95]. We see that the choice of the transducing fluid is crucial to enhance the sensitivity (see Section 2.3). In addition, careful optimization of foci for the two different wavelengths to compensate for geometric and chromatic aberrations is very important to create and detect the maximum allowable signal from the nanoabsorber. We first characterized the sensitivity of our setup with gold nanoparticles used as calibration for estimating absorption cross sections. Their size and shape are well-known. For specific size, shape and local environment, the absorption cross sections of gold nanoparticles are calculated and match measured values.[42,72,128]

Figure 2.4 A shows an image of a sample containing 10 nm and 5 nm diameter gold spheres immersed in glycerol on glass surface. We measured photothermal signals by heating at 514 nm and probing at 800 nm. The signals from different diameters differ by a factor of about 8, as expected from the volume ratio. The elongated shape of the photothermal spots in this image (210 nm and 370 nm principal half-maximum widths) arose from the shape of the pump beam, because spatial filtering was weak in this experiment. Stronger spatial filtering yielded a much better shape (see Fig. 2.4 C and D).

We measured the photothermal detection volume by scanning a 20-nm

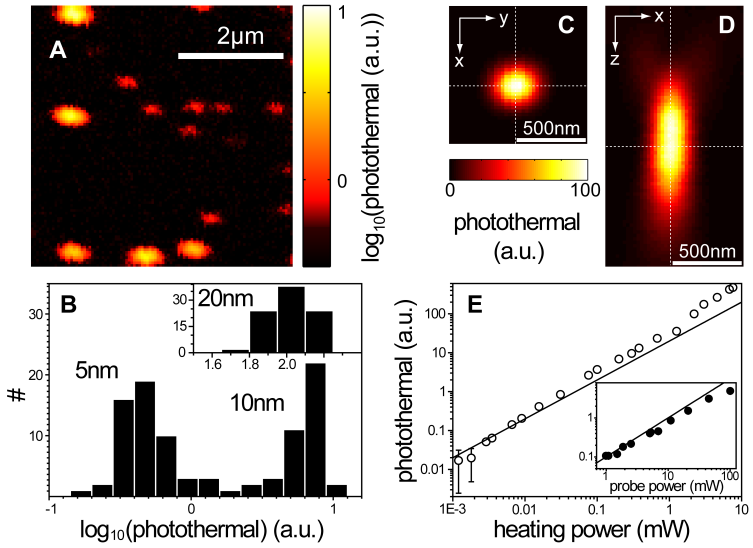

Figure 2.4: Photothermal images of gold nanospheres illustrate the large dynamic range of the method and its low background. (A) A raster scan image of a sample containing 10-nm (yellow) and 5-nm (red) diameter gold particles in glycerol: heating power is 0.43 mW; probe power, 21 mW; integration time per pixel, 3 ms. The FWHMs of the photothermal spots are 210 nm and 370 nm. a.u., arbitrary units. (B) Histogram of the photothermal signals for 94 gold particles of 5-nm or 10-nm diameter. (Inset) Histogram of signals for 88 gold particles of 20-nm diameter in the same conditions. As expected, the photothermal signal roughly scales as the volume of the particles. (C and D) In the case of strong spatial filtering, the point-spread function (PSF) of the photothermal signal is well fitted by a Gaussian with $\sigma_x = 220\ nm$, $\sigma_y = 250\ nm$, and $\sigma_z = 670\ nm$, as mapped by scanning a 20-nm-diameter gold particle in three dimensions. Note the two weak lobes of the PSF in the x, z image, also observed in confocal fluorescence microscopy. (E) Linear scaling of the photothermal signal of a 20-nm gold particle with heating and probe (inset) powers. Solid lines show linear fits at low heating and probe powers. Error bars indicate standard deviation values. For most of the data, they are smaller than the symbol size.

gold sphere in three dimensions.[90] The full widths at half maximum (FWHM, determined by a Gaussian fit) across x, y, and z are 220 nm, 250 nm, and 670 nm, respectively. These data are represented in Fig. 2.4 C and D. Last, we verified the linear relationships between pump and probe powers and photothermal signal by varying the heating power over 4 orders of magnitude

(1 μW to 10 mW) and the probe power over 2 orders of magnitude (1 mW to 100 mW). Slight deviations from linear behavior at high power may be due to variations of spectral or thermal characteristics of the materials in the broad range of temperature changes explored (from 0.05 K up to about 500 K).

2.5.1 Minimum detectable dissipated power

To ascertain the possibility of detecting a single organic molecule in photothermal microscopy, we only need to compare the smallest detectable power over a given integration time to the power dissipated by a single molecule.

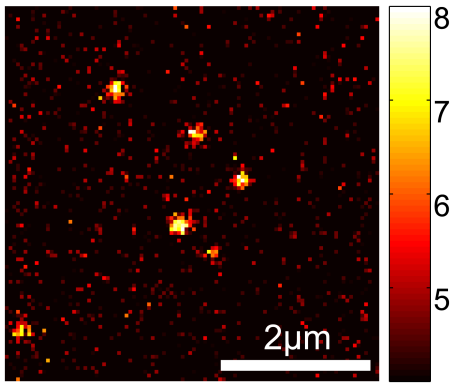

Figure 2.5: Photothermal image of 20 nm gold nanoparticles in glycerol with $P_{heat} = 1$ μW, $P_{probe} = 68$ mW, $\Delta t = 10$ ms. The color scale of photothermal image shows the SNR.

We probe the limits of photothermal detection on 20 nm diameter gold nanoparticles by reducing the dissipated powers as far as possible while having a reasonable SNR of the spots in the image. The result of this experiment is shown in Fig. 2.5. The photothermal spots are obtained when the gold nanoparticles were excited at 514 nm with 1 μW power at the sample. The probe laser power was 68 mW at 800 nm. The average SNR of photothermal spots is 8 with an integration time of 10 ms per pixel.

This way, we experimentally estimate the smallest dissipated power (p_{diss}) and temperature rise (ΔT_{surf}), which we can detect. Under this experimental conditions, we calculated the average dissipated power due to the heating beam as $p_{diss} = 2.6$ nW with a corresponding temperature rise of

$\Delta T_{surf} = 80$ mK.

By increasing the integration time to hundreds of ms, even smaller dissipated powers can be measured.

2.6 Detecting a single molecule by its absorption

A single molecule can release heat along two pathways: a direct nonradiative transition from the excited state and vibronic relaxation before and after a radiative fluorescent transition. The shorter the fluorescence lifetime (τ_F) and the lower the fluorescence quantum yield (η_F) are, the larger is the dissipated power at saturation. The most favorable molecules for photothermal detection should therefore have strong nonradiative channels and thus very weak fluorescence yields. This is the case for the trial molecules chosen in the present work. We calculated the dissipated power at saturation for several commercially available organic molecules (see Appendix A). The highest dissipated power at saturation of 15 nW well above the limit of 3 nW was obtained for a high-efficiency dark quencher (Black-Hole-Quencher, BHQ1, Biosearch Technologies, Novato, California). This azo dye molecule is used in the construct of oligonucleotide probes to quench the fluorescence of a dye in a DNA construct.[129,130] For the present experiments, we first perform absorption measurements on a chromophore-DNA construct to increase the absorption signal by the presence of two chromophores in each construct and to secure the adhesion of the constructs to the glass surface by their single-strand DNA linker (Fig. 2.1). Then we demonstrate the detection of optical absorption at a single molecule level by using single BHQ1-Amine molecules.

2.6.1 Single BHQ1-10T-BHQ1 constructs

A photothermal image obtained on a sample of spin-coated quencher-DNA construct (BHQ1-10T-BHQ1) submerged in nitrogen-bubbled glycerol is shown in Fig. 2.6 A. The image reveals four photothermal spots with a SNR $\sim$ 10 for an integration time of 300 ms. These spots persisted for as long as 1 hour without bleaching or fading. Less than 2% of the molecules bleached in the first 10 min of illumination. When the glycerol was saturated by oxygen, in contrast, one-step photobleaching was observed after an average time of $\sim$ 1 min. Several typical background-corrected photothermal

traces are displayed in Fig. 2.6 B and demonstrate digital irreversible steps. We never observed any blinking or any later reappearance of a bleached photothermal signal.

The absolute value of the change in absorption cross section upon photobleaching is estimated by comparison to the photothermal signal of 20-nm gold nanoparticles. The calculated[42,72] cross section of these gold nanospheres is 460 nm^2 at 514 nm in glycerol, in good agreement with absolute cross section measurements.[128]

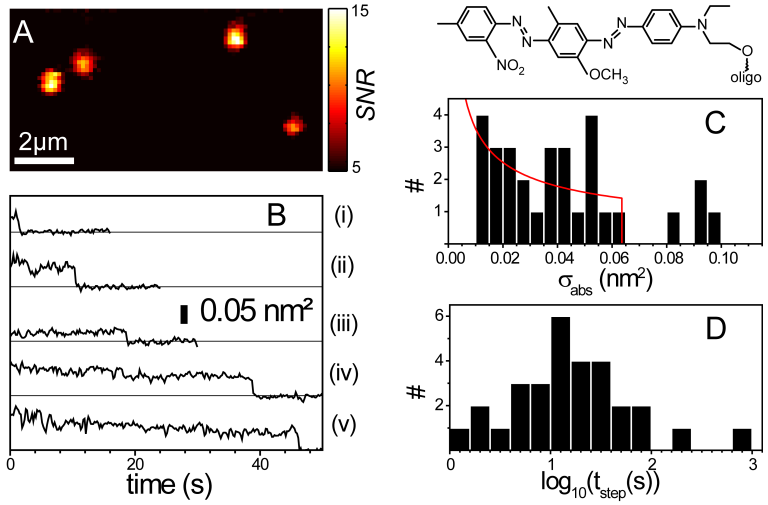

Figure 2.6: (A) Photothermal image of four constructs (BHQ1-10T-BHQ1), consisting of two fluorescence quenchers (BHQ1) attached to a single strand of DNA (10 thymine bases): integration time per pixel, 300 ms; heating power, 5.1 mW at 514 nm; probe power, 84 mW at 800 nm. (B) Photothermal time traces showing single-step bleaching obtained on a sample with BHQ1-10T-BHQ1 on glass in oxygen-saturated glycerol: integration time per point, 100 ms; heating, 5.1 mW; probe, 84 mW. (C) Histogram of amplitude of 30 bleaching steps in the photothermal traces. The average change in absorption cross section upon bleaching is 4.1 $Å^2$. The red line represents the distribution of absorption cross sections of single chromophores corresponding to the isotropic distribution of transition dipole moments. The cutoff at 6.3 $Å^2$ is the calculated cross section for a perfectly oriented molecule. (D) Histogram of survival times before one-step photobleaching events for the same set of data. The average time is 49 s.

The histogram in Fig. 2.6 C summarizes the absorption cross-section changes in 30 single bleaching steps, with an average value of 4.1 $Å^2$. This

value, which corresponds to the cross section of a single chromophore, is in satisfactory agreement with the isotropic value, $\sigma_{BHQ} = 2.1$ Å^2, deduced from the absorption spectrum of the quencher-DNA construct in glycerol. Note that the maximum value of the cross section for a favorably oriented molecule is $3\,\sigma_{BHQ} = 6.3$ Å^2. The histogram of Fig. 2.6 C is a broad distribution without distinct maximum, in qualitative agreement with the isotropic distribution of transition dipole moments (solid line in Fig. 2.6 C with a step-like cutoff at $3\,\sigma_{BHQ}$). Our observation suggests that the absorption dipoles of BHQ1 molecules are not freely rotating, even under the heavy illumination to which we subjected them, and that the molecules are fixed to the surface and/or to the DNA linker.

The histogram of survival times before digital photobleaching is shown in Fig. 2.6 D. The average number of absorbed photons before bleaching is about 10^{11} under oxygen-saturated conditions and larger than 10^{12} under oxygen-free conditions, showing a huge reduction in the bleaching efficiency per photon compared with usual fluorophores in the same conditions. This robustness can be attributed to the much shorter dwell time in the excited singlet state resulting from the efficient internal conversion. We have attempted measurements of the polarization dependence of single-molecule absorption signals, but these measurements were very difficult because of the buildup of a photothermal background over long illumination times by the pump beam (the probe had no noticeable effect on this buildup).

We could not observe simultaneous fluorescence and photothermal signals from the spots of Fig. 2.6. Such simultaneous signals arose only from abnormally bright spots, attributable to large aggregates, and showed quick correlated decays of both signals upon illumination. On the sample of Fig. 2.6, we also observed a few spots with strong photothermal signals corresponding to an absorption cross section of about 1 nm^2, which showed one-step bleaching. Possible interpretations are aggregates of several molecules desorbing simultaneously or, more probably, another chemical species with a large absorption cross section, possibly with excited-state absorption of the intense probe beam. We only found very few examples of two-step photobleaching of the BHQ1-10T-BHQ1 constructs. We believe that this absence results from the low probability of bleaching, joined with the low probability of finding two favorable orientations in the same construct.

2.6.2 Single BHQ1-Amine molecules

We performed the photothermal microscopy experiments on single BHQ1-Amine molecules under similar conditions as with DNA-constructs. The photothermal image of the molecules is shown in Fig. 2.7. The color-scale stands for the SNR and the calculated absorption cross sections σ_{abs}, simultaneously. We could image an arbitrary single BHQ1-Amine molecule with an average absorption cross section of $\sim$3 Å^2 with a signal-to-noise ratio of $\sim$ 11, which is in good agreement with the previously represented performance of the setup. We see a distribution in absorption cross sections which are within the range of isotropic $\sigma_{BHQ} = 2.1$ Å^2 and $3\,\sigma_{BHQ} = 6.3$ Å^2 of a favorably oriented molecule (see section 2.6.1). This observation suggests a similar conclusion as with DNA-constructs, that the molecules are not freely rotating and they are fixed to the substrate.

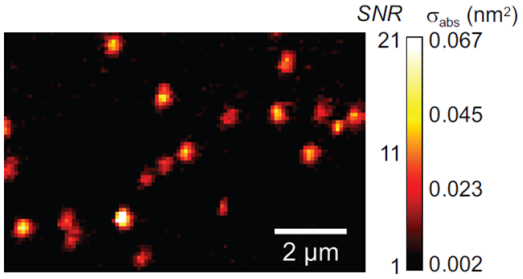

Figure 2.7: Photothermal image of BHQ1-Amine molecules on glass surface in glycerol: integration time per pixel 300 ms, heating power 5.1 mW at 514 nm, probe power 79 mW at 800 nm.

2.7 Conclusions

Our successful single-molecule detection relied here on favorable conditions, the use of glycerol (with large $\partial n/\partial T$ and poor heat conduction) instead of water, with a high heating power of 5.1 mW focused into the diffraction-limited spot and with an even higher probe power of more than 70 mW. Although the conditions for single-molecule absorption in a cell, for example, would be far from these ideal ones, this result opens the way for further optimization of the technique and to a much broader variety of absorbing molecules. Interesting candidates are natural absorbers, for example, metal

proteins such as hemoglobin, which would be useful for applications in analytical biochemistry and medical assays.[131]

An intrinsic limitation of the photothermal method is the low transduction factor between pump and probe because of the relatively weak variation of refractive index with temperature. A future search for more-efficient transduction, for example, photomechanical or photoelectrical detections using micro- and nano-optomechanical systems,[132] appears full of promise.

Acknowledgements

We acknowledge financial support by European Research Council (Advanced Grant SiMoSoMa). This work is a part of the research program of the Stichting voor Fundamenteel Onderzoek der Materie, which is financially supported by the Netherlands Organization for Scientific Research. We thank Harmen van der Meer for precious help with the experimental setup.